Planar Helical Antenna of Circular Polarization

Zhuozhu Chen, *Student Member, IEEE*, and Zhongxiang Shen, *Senior Member, IEEE*

***Abstract*—A planar helical antenna is presented for achieving wideband end-fire radiation of circular polarization while maintaining a very low profile. The helix is formed using printed strips with straight-edge connections implemented by plated via-holes. The currents flowing on the strips and along via-holes of the helix contribute to the horizontal and vertical polarizations, respectively. Besides, the current on the ground plane is utilized to weaken the strong amplitude of the horizontal electric field generated by the one on the strips. Thus, a good circular polarization can be achieved. Furthermore, a tapered helix and conducting side-walls are employed to broaden the axial ratio bandwidth as well as to improve the end-fire radiation pattern. The designed antenna operates at the center frequency of 10 GHz. Simulated results show that the planar helical antenna achieves wide impedance bandwidth ($|S_{11}| < -10$ dB) from 7.4 GHz to 12.8 GHz (54%) and 3 dB axial ratio bandwidth from 8.2 GHz to 11.6 GHz (34%), while retaining a thickness of only $0.11\lambda_0$ at the center frequency. A prototype of the proposed antenna is fabricated and tested. Measured results are in good agreement with simulated ones.**

***Index Terms*— Circular polarization, end-fire, helical antenna, low-profile.**

I. Introduction

CIRCURLARLY polarized (CP) antennas have received extensive attention in modern wireless communication since they can suppress the multipath reflection, avoid the polarization mismatch, and support a flexible alignment for the receiving and transmitting antennas. Many CP antennas have been investigated over past decades such as helical antenna [1], [2], spiral antenna [3], patch antenna [4], [5], crossed dipole antenna [6], etc. Among these reported CP antennas, helical antennas can exhibit CP end-fire radiation, high gain, and wide bandwidth [7], which are in great demand for airborne and space tracking applications. However, traditional helical antennas are not suitable for surface-mounted and space-constrained applications, because their profiles are generally high.

A lot of efforts have been made to design compact and low-profile helical antennas. In [8], a low pitch angle and small number of turns were employed in a helical antenna to realize a low-profile configuration. In [9], a hemispherical helical antenna was proposed to obtain a compact size, low profile as well as CP radiation over a wide angular range. In addition, meander line was utilized in a quadrifilar helical antenna to decrease the total length of the antenna [10]. Although the profiles can be efficiently decreased, these antennas are not planar structures, which may result in aerodynamic drags if they are mounted on moving platforms.

From a practical point of view, a planar helix is a suitable candidate to be well integrated on the surfaces of the installations, and its cross-section can be either square or rectangular. Square helical antennas have been reported to realize circular polarization with end-fire radiation [11]-[13]. In [13], a square helical antenna was integrated into a semiconductor silicon substrate, achieving good CP performance while maintaining the substrate thickness of 0.22 λ_0 at the center frequency. Generally speaking, a rectangular cross-section can further decrease the profile of the planar helical antenna. A rectangular planar helix has found many applications in slow-wave structures [14]-[16] and linearly polarized antennas [17]-[18], but little literature has been reported on CP end-fire antennas so far. It is well known that in order to realize circular polarization, two orthogonal electric fields with equal amplitude and phase difference of 90° are required. For rectangular planar helical antennas, two orthogonal electric fields can be generated by the currents travelling along the perpendicular sides of the helix, respectively. It is expected that if one side of the rectangular is much longer than the other, the amplitudes of two orthogonal electric fields will be of great difference. Therefore, it remains a challenge to achieve CP end-fire radiation for a low-profile planar helical antenna with rectangular cross-section, which may be essential for achieving a low-profile structure.

In this paper, a planar rectangular helical antenna with straight-edge connections implemented by plated via-holes is presented, which is of very low profile and can obtain CP end-fire radiation. Besides the currents flowing along the strips and via-holes of the helix contributing to the horizontal and vertical polarizations, respectively, the current on the inner edge of the ground plane plays an important role in weakening the strong amplitude of the horizontal electric field generated by the current on the strips, which is critical for achieving circular polarization. In addition, tapered helix and conducting side-walls are utilized in the antenna to improve the axial ratio bandwidth and the radiation pattern. The proposed planar helical antenna has the following advantages: 1) The antenna can achieve wide impedance and axial ratio bandwidths. Excellent CP performance with end-fire radiation is obtained over a 34% frequency band. 2) The antenna has a very low profile, which is only $0.11\lambda_0$ at the center frequency. It is very suitable to be mounted on the wings of the unmanned aerial vehicle (UAV) and aircraft. 3) The structure is very simple,

Manuscript received on Feb 28, 2015.

The authors are with the School of Electrical and Electronic Engineering, Nanyang Technological University, 50 Nanyang Avenue, Singapore 639798, (e-mail: chen0855@e.ntu.edu.sg; ezxshen@ntu.edu.sg).

Color versions of one or more of the figures in this letter are available online at http://ieeexplore.ieee.org.

Digital Object Identifier

lightweight, and low-cost. It can be easily fabricated using the printed circuit board technology.

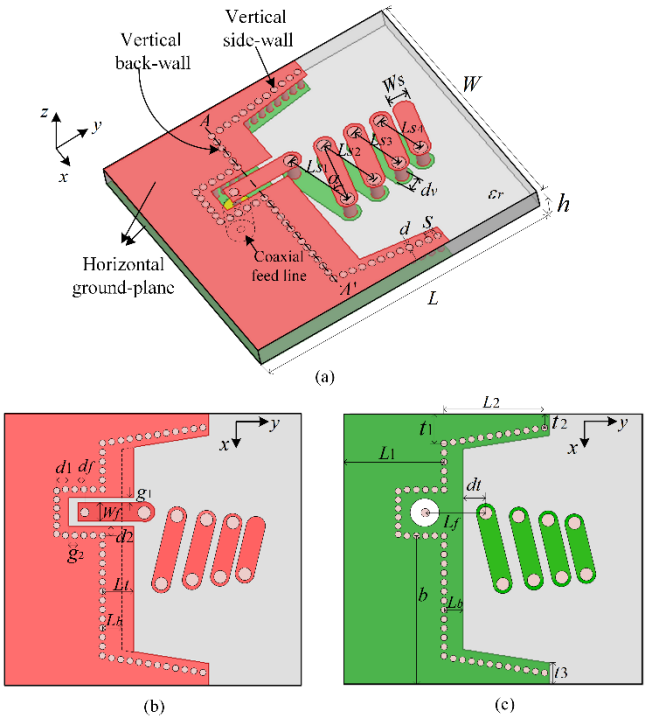

Fig. 1. Configuration of the proposed planar helical antenna, (a) perspective view, (b) top and (c) bottom layers of the substrate.

II. Antenna Configuration

The configuration of the proposed planar helical antenna is shown in Fig. 1. The helix has a rectangular cross-section, which is formed using printed strips with straight-edge connections implemented by plated via-holes. As shown in Fig. 1(a), the length and width of the antenna are denoted by L and W, respectively. ε_r and h represent the dielectric constant and thickness of the substrate, respectively. The diameter of the via hole of the helix is d_v, and the pitch angle between the top and bottom strip is α. The width of each printed strip is uniform, which is represented by W_s. The length of the strip on the bottom layer of the substrate is denoted by L_{si} (i = 1, 2, 3, 4) for the ith turn of the helix. In order to improve the axial ratio and radiation pattern, the helix is tapered according to the following ratio

$$r = \frac{L_{s2}}{L_{s1}} = \frac{L_{s3}}{L_{s2}} = \frac{L_{s4}}{L_{s3}} \tag{1}$$

A coaxial-to-grounded coplanar waveguide (GCPW) transition is employed in the antenna to feed the helix. As shown in Fig. 1(b), W_f is the width of the center strip of the GCPW. g_1 and g_2 represent the gaps between the center strip and its adjacent ground planes. d_f is the distance from the edge of the center strip of the GCPW to the coaxial probe. If a substrate is chosen, the characteristic impedance of the GCPW is determined by the strip width W_f and the gap g_1, while the matching condition from the coaxial probe to the GCPW can be tuned by varying d_f and g_2.

Generally speaking, a large conducting plane which is vertical to the axis of the helix should be incorporated in the helical antenna to obtain a good CP radiation in the end-fire radiation. However, it is not suitable for the low-profile structures. In our proposed antenna, two metallic plates are printed on both the top and bottom layers of the substrate to form the horizontal ground planes. Grounded via-holes with diameter d and spacing s are perforated along the inner edge of the ground planes and around the GCPW, and they satisfy the following criteria [19]

$$0.05\lambda_g < s < 0.25\lambda_g\,, \quad s < 2d \tag{2}$$

to prevent the power from leaking out through the via-gaps, where λ_g is the guided wavelength. These via-holes can be regarded as a small vertical conducting wall of the helical antenna, and they can also help to obtain a good RF ground connection between the top and bottom layers of the substrate and suppress the unwanted parallel-plate waveguide mode. It should be noted that the vertical wall is U-shaped, which consists of the vertical back-wall (AA') and side-walls. The side-walls in the structure can help to increase the gain and to improve the radiation pattern. Furthermore, L_t and L_b in Figs. 1(b) and (c) represent the distances from the vertical back-wall (AA') to the inner edge of the top and bottom grounds, respectively. They can affect the current distribution on the inner edge of the horizontal ground plane.

III. Antenna Analysis

A. One-Turn Helix

The proposed low-profile helical antenna with one-turn helix is designed and analyzed in this part. The substrate used is the Duroid RT 5880 substrate with a relative permittivity of ε_r = 2.2 and thickness of h = 3.175 mm. The strip length of the helix is represented by L_s, the other dimensions are the same as those indicated in Fig. 1. The effective total length of one-turn helix L_{eff} is chosen to be around one free-space wavelength in order to achieve CP radiation in the end-fire direction [12], which can be expressed as

$$L_{eff} = 2\left(h \times \sqrt{\varepsilon_{eff1}} + Ls \times \sqrt{\varepsilon_{eff2}}\right) \approx 1\lambda \tag{3}$$

where $\varepsilon_{eff1} \approx \varepsilon_\gamma$ and $\varepsilon_{eff2} \approx (\varepsilon_\gamma + 1)/2$ [20], [21].

In general, circular polarization is generated by two orthogonal electric fields, which are equal in amplitude and 90° different in phase. For the proposed helical structure, the currents flowing on the strips and along the via-holes of the helix contribute to the horizontal electric field E_ϕ and vertical electric filed E_θ respectively. It is expected that the magnitude of E_ϕ is much stronger than that of E_θ if the height of the via-hole h is very small compared to the strip length L_s, which makes it difficult to meet the criteria of achieving circular polarization. However, in our proposed helical antenna, the current flowing on the inner edge of the ground plane can help to weaken the strong magnitude of E_ϕ generated by the current on the strips. By this way, it is possible to obtain circular polarization in the end-fire direction over a wide frequency range.

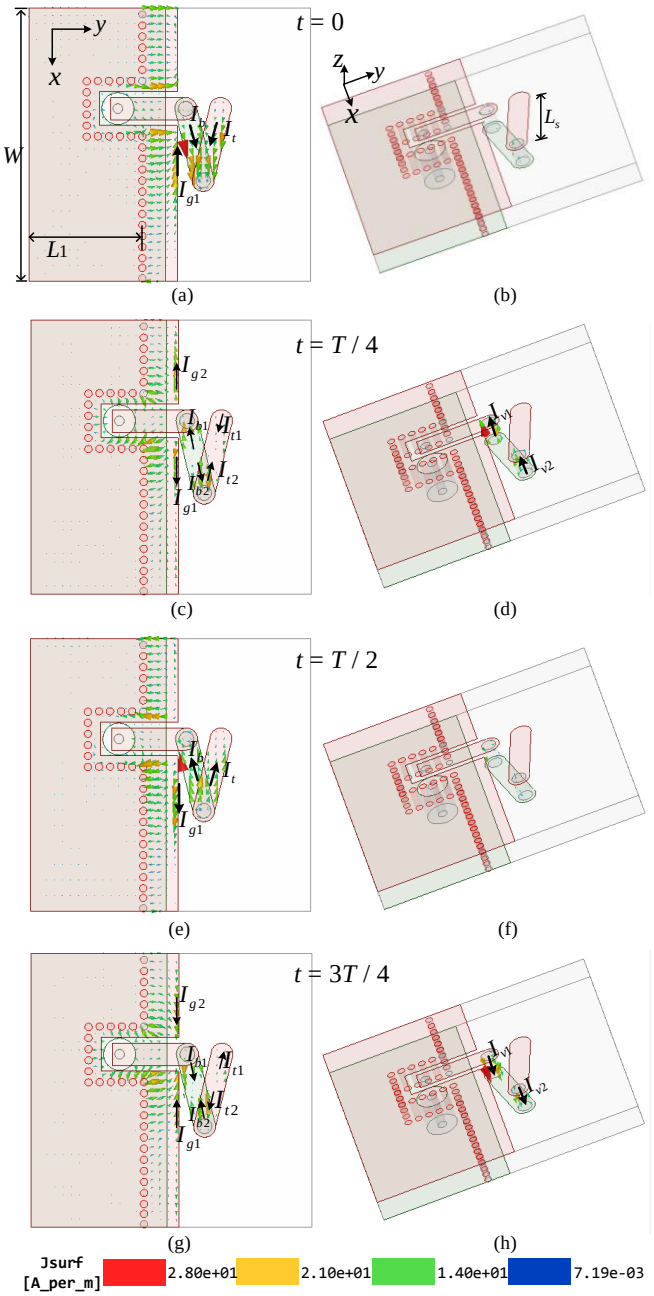

Fig. 2. Current distributions of the low-profile one-turn helical antenna at different times t = 0, T/4, T/2, and 3T/4, where T is the period of time. (a), (c), (e), (g), horizontal currents on the ground plane and strips of the helix, (b), (d), (f), (h) vertical currents along the via-holes of the helix (f = 10 GHz, W = 37 mm, L = 38 mm, h = 3.175 mm, W_s = 3 mm, L_s = 10 mm, α = 28°, d_v = 2 mm, d = 1 mm, s = 1.5 mm, W_f = 3 mm, g_1 = 0.8 mm, g_2 = 1.5mm, d_1 = 1.7 mm, d_2 = 1.4 mm, d_f = 1 mm, L_t = 4.7 mm, L_b = 3.1 mm, L_f = 9.17 mm, d_t = 2.77 mm, L_1 = 15.3 mm, b = 19.6 mm).

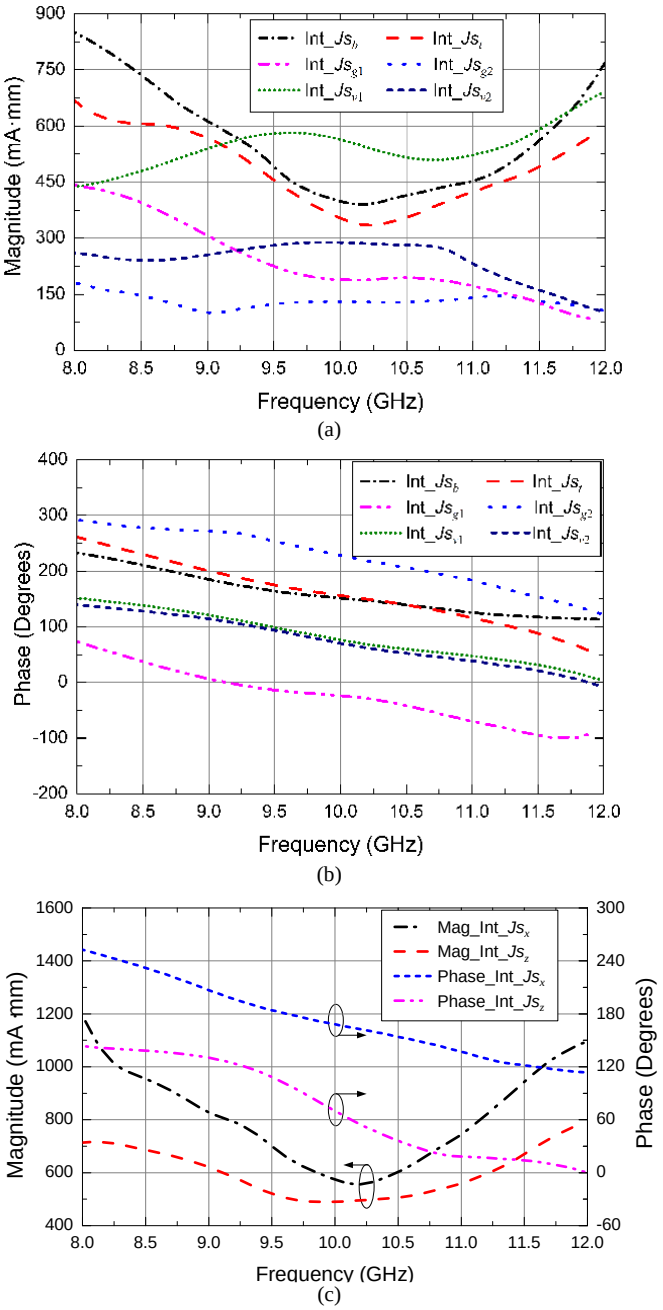

Fig. 3. (a) Magnitude and (b) phase values of surface current density integration of each segment on the helix and edge of the ground, (c) magnitude and phase values of combined total surface current density integrations of x and z directions.

To verify the principle of achieving the circular polarization, the current distribution along the proposed one-turn helical antenna is analyzed with the aid of ANSYS High Frequency Structure Simulator (HFSS), as shown in Fig.2. When t = 0, it is observed from Fig. 2(a) that strong horizontal currents appear on the bottom and top strips, and also on the inner edge of the ground plane, which are denoted by I_b, I_t, and I_{g1}, respectively. On the other hand, the vertical currents flowing along the via-holes are very small, as shown in Fig. 2(b). Therefore, it is concluded that E_ϕ is dominated along the end-fire direction in the far-field region. It should be mentioned that I_{g1} is $-x$ directed, which is opposite to the $+x$ direction of I_b and I_t, so that it can somehow weaken the strong amplitude of E_ϕ generated by I_b and I_t. This is critical for achieving circular polarization, as mentioned earlier. Figs. 2(c) and (d) show the current distributions at $t = T/4$, where T is the period of time. It is seen that strong vertical currents I_{v1} and I_{v2} flow along the via-holes of the helix in the +z direction, while the horizontal currents, as indicated in Fig. 2(c) are weak compared to I_{v1} and I_{v2}. In addition, the currents either on the edge of the ground plane or the strips exhibit two components that are 180° out of phase, so that E_ϕ is very small and E_θ dominates in the far field. The same phenomenon is observed in Figs. 2(e)-(h). As seen,

the current distributions at $t = T/2$, and $t = 3T/4$ are opposite to those when $t = 0$ and $t = T/4$, which also generate the dominant but out-of-phase E_ϕ and E_θ, respectively. As a result, left-hand circular polarization in the end-fire direction can be obtained under the combined influences of the current distributions along the helix as well as on the ground plane of the proposed antenna.

It is well known that the electric field in the far-field is determined by integrating the surface current densities over the distributed areas, which can be represented as [22]

$$\boldsymbol{E}_i \approx -j\frac{\omega\mu}{4\pi}\iint \boldsymbol{J}s_i \frac{e^{-jkR_i'}}{R_i} dS_i \qquad (4)$$

where i represents each segment on the helix and the edge of the ground for our one-turn helical antenna. These segments include the bottom and top strips, the ground edges on each side of the CPW, and two via holes, which are denoted by b, t, $g1$, $g2$, $v1$, and $v2$, respectively. S_i denotes the surface area of segment i, and $\boldsymbol{J}s_i$ is the surface current density distributed on S_i. k is the wavenumber. R_i and R_i' are the distances from the current source to the far-field for amplitude and phase terms, respectively. It is noticed that if we assume that there are no amplitude and phase differences between each current source to the far-field region, the ratio of the horizontal E-field and vertical E-filed approximately equals to that of the combined total integrations of surface current densities over the distributed areas of x component $\iint \boldsymbol{J}s_x\, dS$ and z component $\iint \boldsymbol{J}s_z\, dS$ in the end-fire direction. With the aid of the fields calculator of HFSS, the magnitude and phase values of surface current density integration of each segment on the helix and the edge of the ground are plotted in Figs. 3(a) and (b). We use Int_Js_i ($i = b, t, g1\ldots$) to represent the integration of surface current density over the area of each segment. The input power is set as 1 Watt. As shown, Int_Js_b and Int_Js_t are almost in-phase, which are nearly 180° out-of-phase with Int_Js_{g1} near the center frequency of 10 GHz. In addition, Int_Js_{v1} and Int_Js_{v2} are almost in-phase, which have phase difference around 90° with Int_Js_b and Int_Js_t near the center frequency. These phenomena are in accord with the current distribution displayed in Fig. 2. The magnitude and phase values of the x and z components of the combined total surface current density integrations are also depicted in Fig. 3(c). It is seen that the magnitudes of x and z components are very close, and the phase difference is around 90° near the center frequency of 10 GHz. It is worth noting that no phase differences between each current source to the far-field region is assumed for the analysis in order to basically clarify the physical concept of achieving circular polarization. By taking the phase variations into account, the magnitude ratio and phase difference between the horizontal electric field E_ϕ and vertical electric field E_θ, and axial ratio of the proposed one-turn helical antenna in the end-fire direction are plotted in Fig. 4. It is seen that the magnitude ratio of E_ϕ and E_θ is close to one and the phase difference between two orthogonal fields is almost 90° near the center frequency of 10 GHz. Resultantly, a good circular polarization in the end-fire direction is obtained and the 3 dB AR bandwidth ranges from 9.6 GHz to 10.45 GHz.

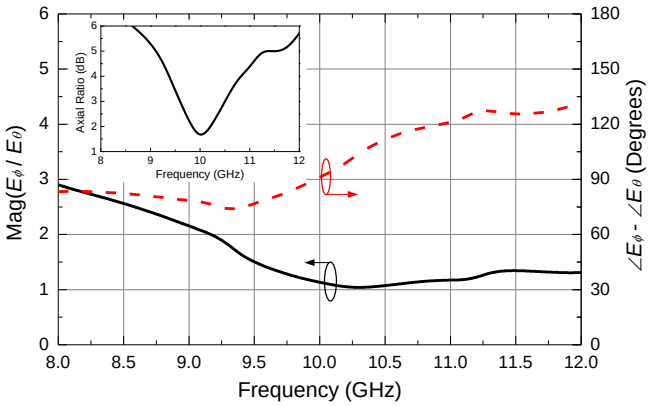

Fig. 4. Simulated magnitude ratio and phase difference of the horizontal electric field E_ϕ and vertical electric field E_θ, and axial ratio of the proposed one-turn helical antenna in the end-fire direction.

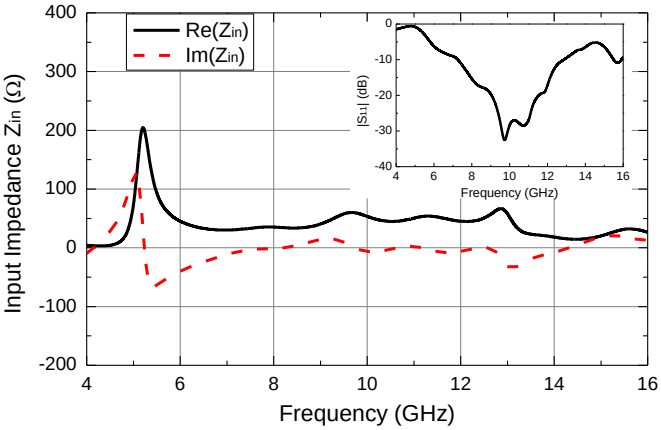

Fig. 5. Simulated input impedance and $|S_{11}|$ of the proposed one-turn helical antenna.

Additionally, it should be noted that the vertical conducting wall made up of via-holes can prevent the power from leaking out through the via-gaps. Resultantly, the current flowing on the ground plane outside the vertical wall is very small. Therefore, the ground length L_1 starting from the wall to the left edge of the substrate and the ground width W, as shown in Fig. 2(a), are of insignificance to the antenna performance, which makes the proposed antenna suitable to be mounted on a large conducting platform.

Furthermore, the helical antennas can achieve wide bandwidths when they operate in the axial mode. This is because the helical antenna is a travelling-wave structure; the outgoing current at the input end and the reflected current at the open end of the helix decays rapidly [7]. In our proposed structure, a coaxial-to-GCPW transition is employed to feed the antenna. By choosing proper parameters W_f, g_1, g_2, and d_f, a good impedance match can be obtained. Fig. 5 shows the simulated input impedance and reflection coefficient $|S_{11}|$ of the proposed one-turn helical antenna. It is seen that the input impedance can maintain a small variation within a wide frequency range, and the 10 dB return loss bandwidth is from 7.2 GHz to 12.5 GHz.

B. Parametric Study

A parametric study is conducted in order to examine the effects of the key parameters on the radiation performance and

help to facilitate the practical design of the proposed low-profile planar helical antenna. The important parameters include: the number of helical turns N, the length of the strip L_s, the pitch angle between the top and bottom strips α, the distances from the vertical back-wall to the inner edge of the top ground L_t and bottom ground L_b, and the strip-length ratio r. Other parameters such as the width of the strip W_s and the diameter of the via hole d_v are of less importance although they also slightly affect the radiation performance, and they will not be discussed in detail below. In the parametric study, only one parameter is varied at one time while the others remain unchanged as follows: W = 40 mm, L = 60 mm, h = 3.175 mm, W_s = 3 mm, d_v = 2 mm, d = 1 mm, s = 1.5 mm, W_f = 2.2 mm, g_1 = 0.6 mm, g_2 = 2mm, d_1 = 2 mm, d_2 = 1.5 mm, d_f = 1.1 mm, L_f = 8.75 mm, d_t = 2.25 mm, L_1 = 17.5 mm, and b = 22 mm.

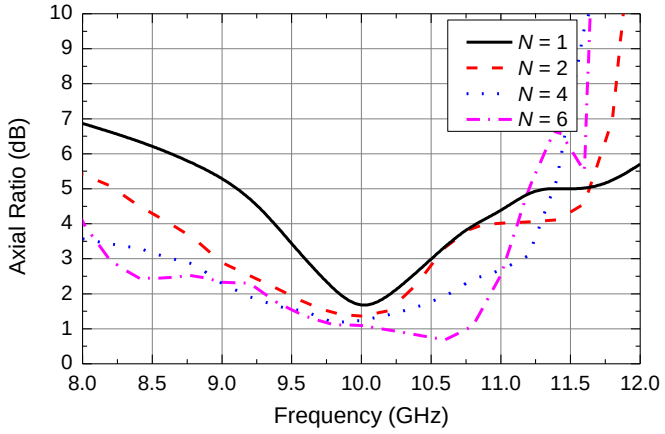

Fig. 6. Effects of the number of turns N on the axial ratio of the proposed helical antenna (L_s = 10.5 mm, $\alpha = 28^o$, L_t = 4 mm, L_b = 2.3 mm).

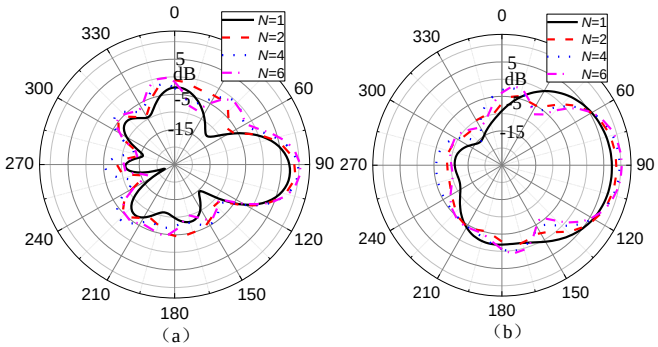

Fig. 7. Effects of the number of turns N on the radiation pattern of the proposed helical antenna *at* f = 10 GHz, (a) *xy*-plane, (b) *yz*-plane (L_s = 10.5 mm, $\alpha = 28^o$, L_t = 4 mm, L_b = 2.3 mm).

1) Number of Turns N

Basically, the helical antenna can achieve better circular polarization performance and higher gain if more turns of helix are employed. Figs. 6 and 7 show the effects of the number of turns N on the axial ratio (AR) and radiation pattern of the proposed antenna, respectively. It is seen the fractional AR bandwidths (AR ≤ 3 dB) are 8.5%, 16%, 26%, and 28.3% for N = 1, 2, 4, and 6, respectively. In addition, the gain values at the center frequency f = 10 GHz are 6.2 dB, 6.9 dB. 7.3 dB, and 7.5 dB for N = 1, 2, 4, and 6, respectively. These results indicate that although the axial ratio bandwidth and gain can be both enhanced with the increase of N, the improvement is small when N is larger than 4. This is due to the fact that the current decays when it travels along the helix [8]. When N is large, the current along the last few turns of the helix is small, slightly contributing to the performance of the antenna. Based on this study, we choose N = 4 in our proposed structure.

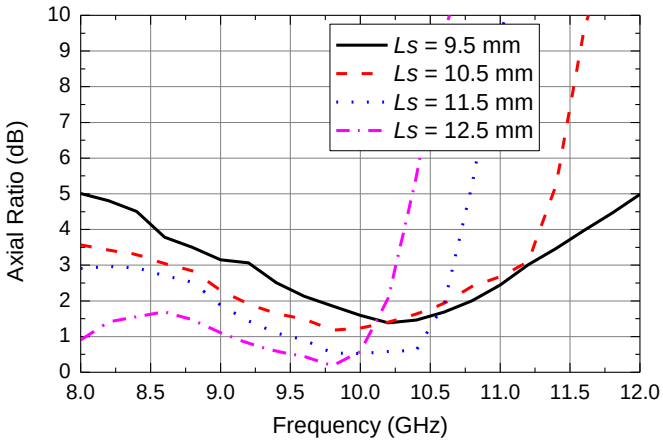

Fig. 8. Effects of the strip length L_s on the axial ratio of the proposed helical antenna (N = 4, $\alpha = 28^o$, L_t = 4 mm, L_b = 2.3 mm).

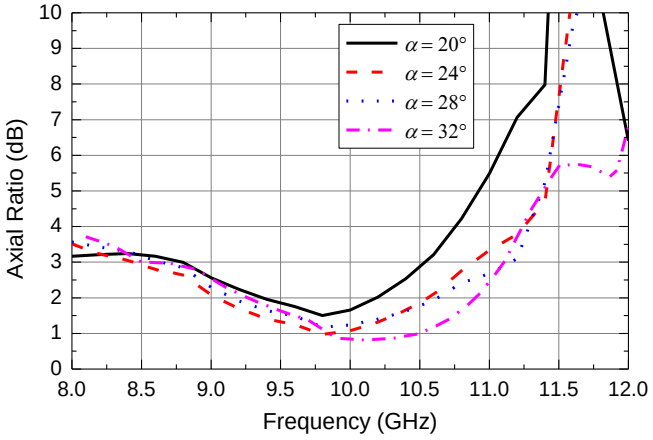

Fig. 9. Effects of the angle α on the axial ratio of the proposed helical antenna (N = 4, L_s = 10.5 mm, L_t = 4 mm, L_b = 2.3 mm).

2) Strip Length L_s

As mentioned earlier, the effective circumference of a helix L_{eff} should be around one free-space wavelength in order to achieve CP radiation in the end-fire direction. Therefore, the strip length L_s is a key parameter to determine the operating frequency band of circular polarization if the substrate thickness is fixed. The effect of L_s on the axial ratio of the proposed helical antenna is shown in Fig. 8. It is observed that the 3 dB axial ratio frequency band shifts to a lower one as the length L_s increases. When L_s = 10.5 mm, the 3 dB axial ratio bandwidth can cover from 8.6 GHz to 11.2 GHz.

3) Pitch Angle α

The pitch angle α plays an important role on the current distribution on the top and bottom strips so that it can affect the axial ratio of the proposed helical antenna. As shown in Fig. 9, the 3 dB AR bandwidth is 12.5% for a small angle $\alpha = 20^o$, and it can be enhanced by increasing the value α appropriately. When the angle $\alpha = 28^o$ and $\alpha = 32^o$, the AR bandwidths are both around 26%. On the other hand, it should be mentioned the

gain values in the end-fire direction are 7.6 dB, 7.4 dB. 7.3 dB, and 7 dB for α = 20°, 24°, 28°, and 32°, respectively, which indicates that a larger α may slightly degrade the gain of the antenna. This is due to the fact that the current flowing on the strips can be divided into *x*-directed and *y*-directed components, a larger α results in an increase of the *y*-directed component and decrease of the *x*-directed one, which can enhance the sidelobe of the radiation pattern and reduce the gain in the +y direction. Therefore, taking both axial ratio and gain into account, we choose $\alpha = 28^{o}$ in the proposed antenna.

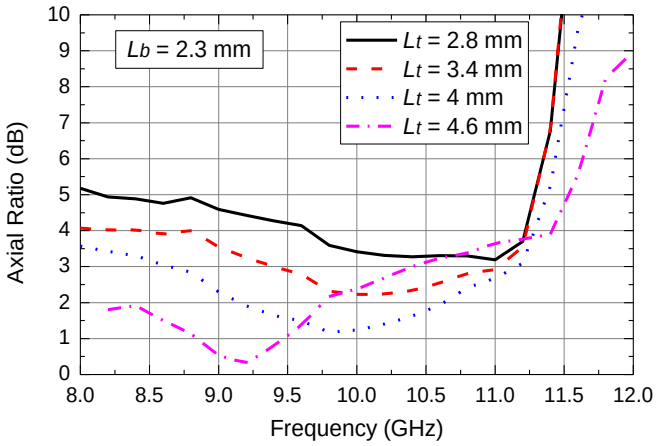

(a)

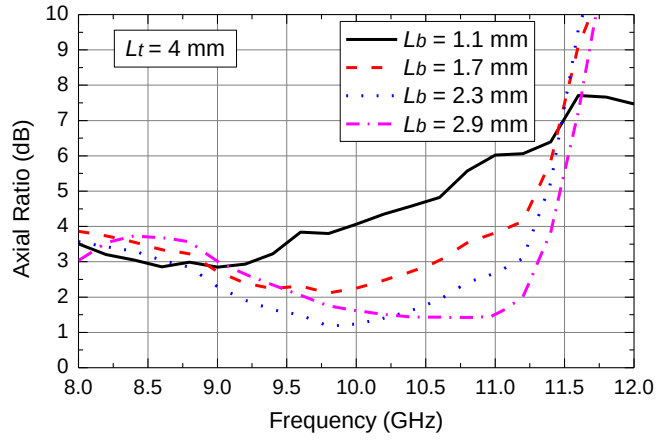

(b)

Fig. 10. Effects of the distance (a) L_t and (b) L_b on the axial ratio of the proposed helical antenna (N = 4, L_s = 10.5 mm, $\alpha = 28^{o}$).

4) Distances Lt and Lb

The distances L_t and L_b exhibit significant effects on AR performance of the antenna since they can influence the current distributions on the inner edge of the top and bottom ground planes. As shown in Fig. 10, it is found that the AR values of the antenna are sensitive to the variations of L_t and L_b, and the best AR performance of the proposed structure with four-turn uniform helix can be obtained when L_t = 4mm and L_b = 2.3mm. Therefore, the values of L_t and L_b should be carefully optimized in order to achieve good CP performance.

5) Strip-Length Ratio r

The significance of the strip-length ratio *r* on the antenna's AR performance is shown in Fig. 11. In the parametric study, the length of the first strip L_{s1} is kept as 12.5 mm, and the pitch angle is maintained as $\alpha = 28^{o}$. The planar helix is uniform when *r* =1, and is tapered as *r* decreases. It is seen that the values of the AR at higher frequencies are improved and the AR bandwidth is enhanced when the helix gradually tapers. The best AR performance of the proposed structure is obtained when *r* = 0.89. It should also be noted that *r* cannot be too small to avoid the overlapping of both edge ends of printed strips.

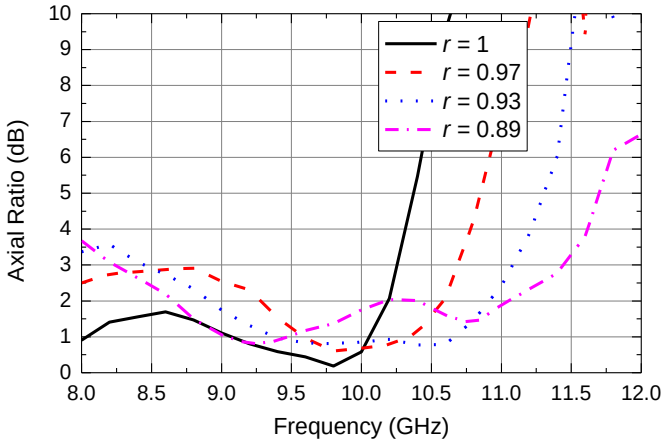

Fig. 11. Effects of the strip-length ratio *r* on the axial ratio of the proposed helical antenna (N = 4, L_{s1} = 12.5 mm, $\alpha = 28^{o}$, L_t = 4 mm, L_b = 2.3 mm).

C. Effects of the Tapered Helix and Conducting Side-Wall

The radiation pattern of the antenna can be improved by utilizing tapered helix and conducting side-walls. Fig. 12 shows the simulated radiation patterns in the xy-plane and yz-plane of three antenna designs, which include Ant. #1: uniform helix without side-wall, Ant. #2: tapered helix without side-wall, and Ant. #3: tapered helix with side-walls. It is seen that the sidelobe levels (SLLs) of the radiation patterns of Ant. #1 are relatively high. In comparison, by tapering the helix as Ant. #2, the SLLs are improved and the gain values increase accordingly at higher frequencies. Furthermore, comparing the radiation patterns of Ant. #3 and Ant. #2, it is concluded that employing side-walls can further enhance the gain and improve the SLLs of the proposed antenna. Besides the radiation patterns, the AR values of the three antennas are compared in Fig. 13. It is observed that the AR bandwidths of Ant. #2 and Ant. #3 are almost the same, and they are wider than that of Ant. #1. Therefore, tapered helix and conducting side-walls are both employed in our final design considering the improvement of AR, antenna gain as well as the radiation pattern.

IV. Experimental Verification

A prototype is fabricated to characterize the performance of the proposed planar helical antenna, as shown in Fig. 14. The substrate used in this design is Duroid RT 5880 substrate with permittivity of 2.2, loss tangent of $\tan\delta = 0.0009$, and thickness of 3.175 mm. The outer conductor of a 50 Ω SMA connector is soldered on the bottom layer of the substrate, the inner conductor is connected to the center strip of the GCPW to feed the antenna. For the matching purpose, the center strip width of the GCPW is designed to be W_f = 3 mm, the gaps between the center strip and its adjacent ground planes are g_1 = 0.8 mm and g_2 = 1.5 mm, respectively. The distance from the edge of the center strip of the GCPW to the coaxial probe is d_f =

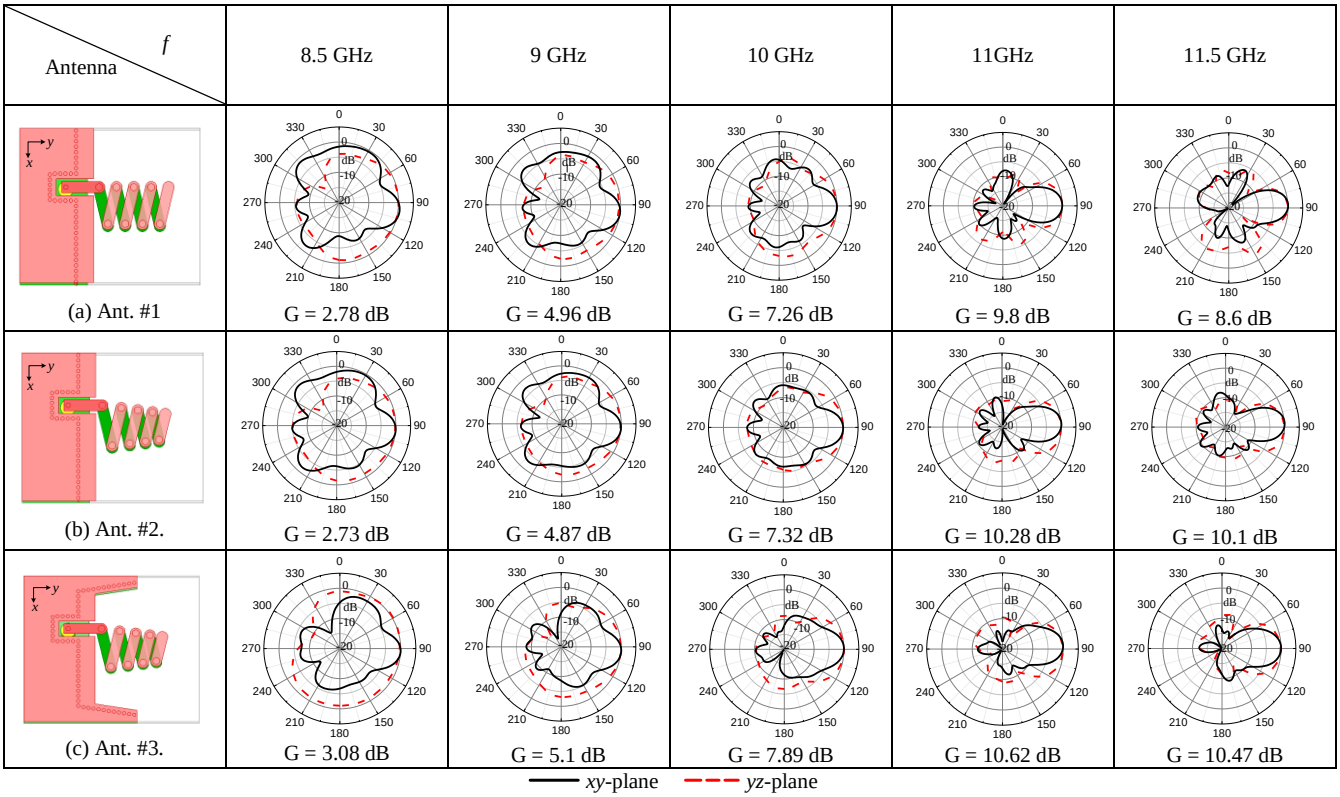

Fig. 12. Radiation pattern comparison of three planar helical antenna designs at different frequencies. (a) Ant. #1: uniform helix without side-wall (r = 1, L_{s1} = 10.5 mm), (b) Ant. #2: tapered helix without side-wall (r = 0.89, L_{s1} = 12.5 mm), and (c) Ant. #3: tapered helix with side-walls (r = 0.89, L_{s1} = 12.5 mm).

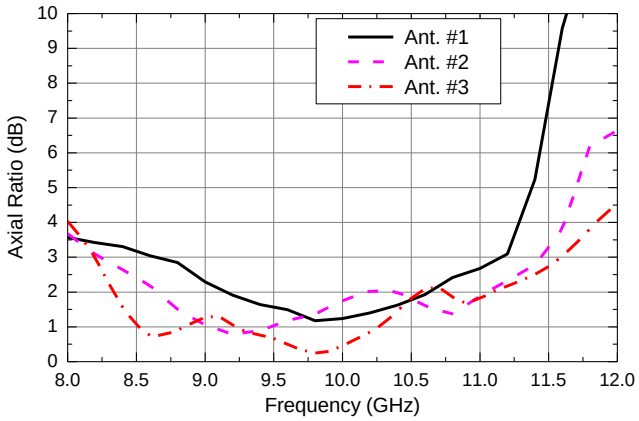

Fig. 13. Simulated axial ratio values of three planar helical antenna designs. (Ant. #1: uniform helix without side-wall, Ant. #2: tapered helix without side-wall, and Ant. #3: tapered helix with side-walls.)

1.2 mm. The corresponding characteristic impedance of the GCPW is 73.1 Ω. Based on the analysis conducted in Section III, the other dimensions are: W = 44 mm, L = 52 mm, W_s = 3.2 mm, L_{s1} = 12.5 mm, r = 0.89, $\alpha = 28°$, d_v = 2 mm, d = 1 mm, s = 1.5 mm, d_1 = 1.83 mm, d_2 = 1.45 mm, L_t = 4.9 mm, L_b = 3.2 mm, L_f = 9.66 mm, d_t = 1.86 mm, b = 24.32 mm, L_1 = 15.9 mm, L_2 = 16.3 mm, t_1 = 4.67 mm, t_2 = 2.13 mm, t_3 = 3.5 mm.

S parameter of the proposed antenna is measured using a calibrated Agilent vector network analyzer N5230A. The comparison between the simulated and measured $|S_{11}|$ is shown in Fig. 15. It is seen that the 10 dB return loss bandwidth ranges from 7.4 GHz to 12.8 GHz for the simulated result, and from 7.2 GHz to 12.9 GHz for the measured one. The corresponding

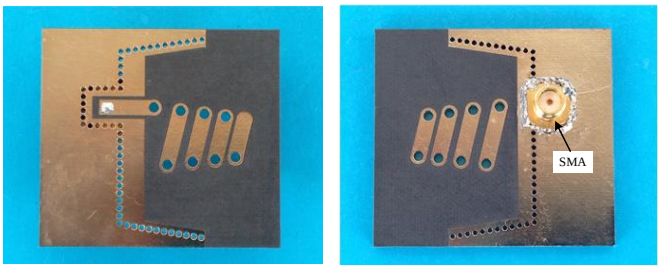

Fig. 14. Prototype of the proposed planar helical antenna. (a) Top view, (b) bottom view.

fractional bandwidths are 54% and 57%, respectively. The slight difference may be due to the fabrication tolerance. Axial ratio and radiation pattern of the proposed antenna are measured in an anechoic chamber. Fig. 16 shows the simulated and measured axial ratio values in the end-fire direction. Simulated result indicates that a 3 dB axial ratio bandwidth of 34% can be achieved for the proposed antenna, which covers from 8.2 GHz to 11.6 GHz. The measured result agrees well with the simulated one. The simulated and measured radiation patterns in the *xy*-plane and *yz*-plane at different frequencies are depicted in Fig. 17. As seen, end-fire radiations are obtained over the frequency range from 8.5 GHz to 11.5 GHz, simulated and measured results are in good agreement as well. It is noted that the radiation patterns are not very symmetric respect to end-fire direction, which is due to the asymmetry of the structure. In addition, the sidelobe level (SLL) and front-to-back ratio (F/B) are relatively high at the lowest frequency of f = 8.5 GHz. Two reasons may account for this

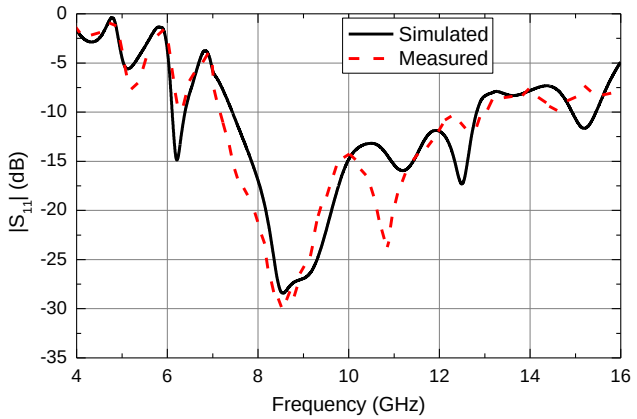

Fig. 15. Simulated and measured $|S_{11}|$ results of the proposed antenna.

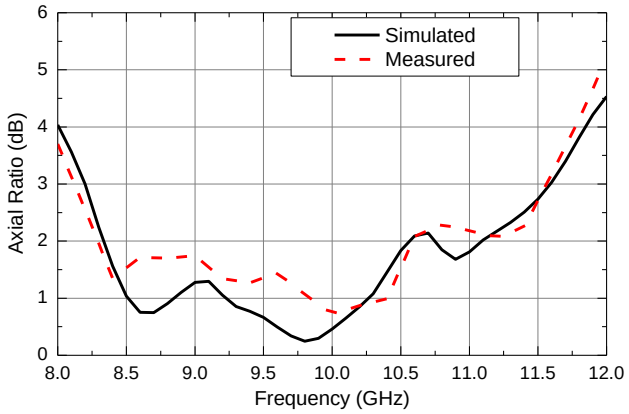

Fig. 16. Simulated and measured axial ratio of the proposed antenna.

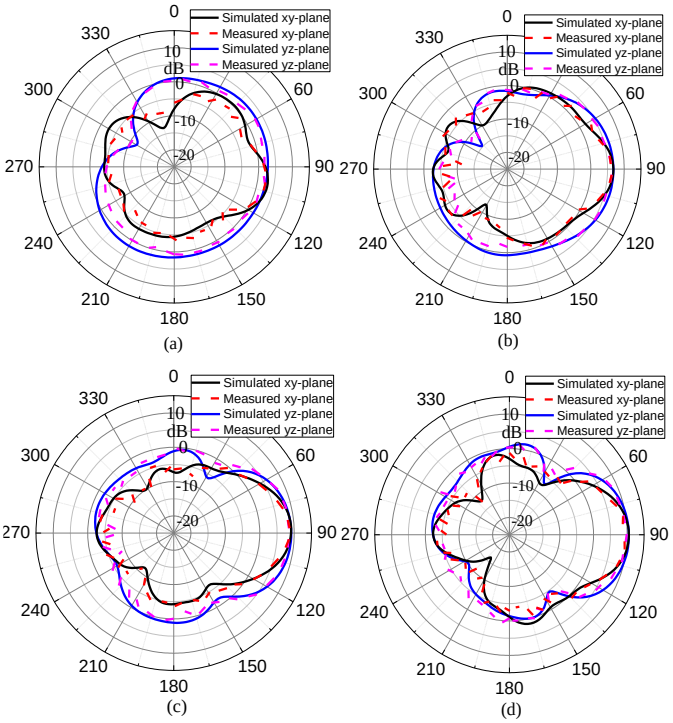

Fig. 17. Simulated and measured radiation patterns of the proposed antenna at different frequencies. (a) 8.5 GHz, (b) 9.5 GHz, (c) 10.5 GHz, (d) 11.5 GHz.

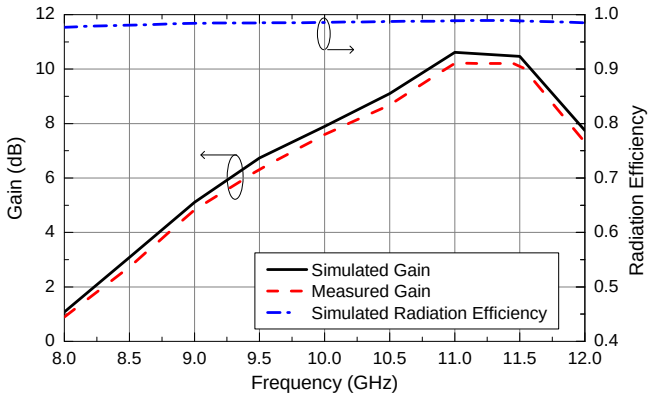

Fig. 18. Simulated and measured gain values and simulated radiation efficiency of the proposed antenna.

phenomenon. First, the normal mode of the helical antenna may appear at the lowest frequency, which can distort the radiation pattern of the axial mode. Second, it is well known that a large conducting wall vertical to the axis of the helix is generally employed in the traditional helical antennas to improve the SLL and *F*/*B*. However, our structure only employs a small vertical via-wall rather than a large one for the sake of low profile. The height of the vertical wall is very small compared to the operating wavelength, which degrades the radiation pattern, especially at lower frequencies. In addition, the simulated and measured gain values in the end-fire direction are depicted in Fig. 18. The simulated gain is 3.1 dB at 8.5 GHz, and increases to 10.5 dB at 11.5 GHz. At frequencies lower than 8.5 GHz and higher than 11.5 GHz, the gain decreases with the degradation of the end-fire radiation patterns. The measured gain values are slightly less than the simulated ones. This discrepancy may be due to the additional loss introduced by the SMA connector and the alignment error of the measurement setup. Furthermore, it should be mentioned that perfect electric conductors are assumed in the simulated model. By taking the loss of the substrate into account, the simulated radiation efficiency is also plotted in Fig. 18. It is seen that the proposed antenna achieves a very high radiation efficiency.

Table I summaries the performance comparison of existing low-profile helical antennas. It is seen that although the antennas in [17] and [18] retain much lower thickness than the others, they achieve linear polarization only. Compared to the other circularly polarized low-profile helical antennas, our proposed antenna clearly exhibits the overwhelming advantages in terms of impedance and AR bandwidths as well as the antenna thickness. In addition, our proposed planar helical antenna is very simple and is suitable for mass production with low cost.

V. Conclusion

In this paper, a low-profile planar helical antenna with straight-edge connections implemented by plated via-holes has been presented for CP end-fire radiation. The operating principle of achieving circular polarization has been analyzed based on the current distribution of the proposed antenna with one-turn helix. Parametric studies have been conducted to analyze the influences of the key parameters on the antenna performance. In addition, the effects of the tapered helix and conducting side-walls on the radiation pattern and axial ratio have been studied. Wide impedance and AR bandwidths and

TABLE I
PERFORMANCE COMPARISON OF EXISTING LOW-PROFILE HELICAL ANTENNAS

Ref.	Structure	Impedance Bandwidth ($\|S_{11}\|$ < -10 dB)	AR Bandwidth (AR <3 dB)	Height (λ_0 is the wavelength at the center frequency)	Gain at the center frequency (dB)	Polarization	Fabrication Complexity
[8]	Non-planar	-	12%	0.19 λ_0	9	Circular	Medium
[9]	Non-planar	-	14.6%	~0.15 λ_0	9.2	Circular	Complex
[13]	Planar	20.5%	Narrow	0.22 λ_0	-	Circular	Medium
[17]	Planar	15%	-	0.02 λ_0	-	Linear	Simple
[18]	Planar	6.1%	-	0.013 λ_0	0	Linear	Simple
Our work	Planar	54%	34%	0.11 λ_0	8	Circular	Simple

excellent CP end-fire performance have been verified by experimental measurements. It is worth mentioning that the proposed planar helical antenna is of very low profile and low cost, and can be readily extended to array configurations.

REFERENCES

[1] H. A. Wheeler, "A helical antenna for circular polarization," *Proc. IRE*, vol. 35, no. 12, pp. 1484–1488, Dec. 1947.

[2] J. M. Tranquilla and S. R. Best, "A study of the quadrifilar helix antenna for global positioning system (GPS) applications," *IEEE Trans. Antennas Propag.*, vol. 38, no. 10, pp. 1545–1550, Oct. 1990.

[3] H. Nakano, H. Oyanagi, and J. Yamauchi, "A wideband circularly polarized conical beam from a two-arm spiral antenna excited in phase," *IEEE Trans. Antennas Propag.*, vol. 59, no. 10, pp. 3518–3525, Oct. 2011.

[4] J. Huang, "Microstrip antenna developments at JPL," *IEEE Antennas Propag. Mag.*, vol. 33, no. 3, pp. 33–41, Jun. 1991.

[5] Y. M. Pan, S. Y. Zheng, and B. J. Hu, "Wideband and low-profile omnidirectional circularly polarized patch antenna," *IEEE Trans. Antennas Propag.*, vol. 62, no. 8, pp. 4347–4351, Aug. 2014.

[6] J. W. Baik, K. J. Lee, W. S. Yoon, T. H. Lee, and Y. S. Kim, "Circularly polarised printed crossed dipole antennas with broadband axial ratio," *Electron. Lett.*, vol. 44, no. 13, pp. 785–786, Jun. 2008.

[7] D. J. Kraus and R. J. Marhefka, *Antennas: For All Applications*, 3rd ed. New York: McGraw-Hill, 2002

[8] H. Nakano, H. Takeda, T. Honma, H. Mimaki, and J. Yamauchi, "Extremely low-profile helix radiating a circularly polarized wave," *IEEE Trans. Antennas Propagat.*, vol. 39, no. 6, pp. 754–757, Jun. 1991.

[9] H. T. Hui, K. Y. Chan, and E. K. N. Yung, "The low-profile hemispherical helical antenna with circular polarization radiation over a wide angular range," *IEEE Trans. Antennas Propagat.*, vol. 51, no. 6, pp. 1415–1418, Jun. 2003.

[10] M. G. Ibambe, Y. Letestu, and A. Sharaiha, "Compact printed quadrifilar helical antenna," *Electron. Lett.*, vol. 43, no. 13, pp. 697–698, 2007.

[11] H. L. Knudsen, "Radiation field of a square, helical beam antenna," *J. Appl. Phys.*, vol. 23, no. 4, pp. 483-491, Apr. 1952.

[12] J. P. Casey and R. Bansal, "Square helical antenna with a dielectric core," *IEEE Trans. Antennas Propag.*, vol. 30, no. 4, pp. 429–436, Nov. 1988.

[13] N. Somjit and J. Oberhammer, "Three-dimensional micromachined silicon-substrate integrated millimeter-wave helical antennas," *IET Microw. Antennas Progag.*, vol. 7, no. 4, pp. 291-298, Jan. 2013.

[14] C. Chua, S. Aditya, and Z. Shen, "Planar helix with straight-edge connections in the presence of multilayer dielectric substrates," *IEEE Trans. Electron Devices*, vol. 57, no. 12, pp. 3451–3459, Dec. 2010.

[15] S. Aditya and R. K. Arora, "Guided waves on a planar helix," *IEEE Trans. Microw. Theory Tech.*, vol. 27, no. 10, pp. 860–863, Oct. 1979.

[16] C. F. Fu, Y. Y. Wei, W. X. Wang, and Y. B. Gong, "Dispersion characteristics of a rectangular helix slow-wave structure," *IEEE Trans. Electron Devices*, vol. 55, no. 12, pp. 3582–3589, Dec. 2008.

[17] H. Ma and H. Y. D. Yang, "Miniaturized integrated folded helical antennas" *in Proc. IEEE Antennas Propag. Soc. Int. Symp.*, Jul. 2011, pp. 753–756.

[18] D. Seo, Y. Yu, S. Jeon, and J. Choi, "An integrated two-wire helical antenna for Bluetooth application", *in Proc. IEEE Antennas Propag. Soc. Int. Symp.*, Jun. 2007, pp. 3552–3555.

[19] D. Deslandes and K. Wu, "Accurate modeling, wave mechanisms, and design considerations of a substrate integrated waveguide," *IEEE Trans. Microw. Theory Tech.*, vol. 54, no. 6, pp. 2516-2526, Jun. 2006.

[20] L. C. Kuo and H. R. Chuang, "A study of printed dipole antennas for wireless communication applications," *J. Electromagn. Waves Appl.*, vol. 21, no. 5, pp. 637–652, Jan. 2007.

[21] K. G. Thomas and G. Praveen, "A novel wideband circularly polarized printed antenna," *IEEE Trans. Antennas Propag.*, vol. 60, no. 12, pp. 5564–5570, Dec. 2012.

[22] C. A. Balanis, *Antenna Theory Analysis and Design*, 3rd ed. New York: Wiley, 2005.

Zhuozhu Chen (S'13) was born in Hunan, China. He received the B.Eng. degree and the M.S. degree in electric engineering from Beijing Institute of Technology, China, in 2010 and 2013, respectively. He is currently working toward the Ph.D. degree in electrical and electronic engineering at Nanyang Technological University, Singapore.

His research interests include design of RF/microwave antennas and circuit.

Zhongxiang Shen (M'98-SM'04) received the B. Eng. degree from the University of Electronic Science and Technology of China, Chengdu, China, in 1987, the M. S. degree from Southeast University, Nanjing, China, in 1990, and the PhD degree from the University of Waterloo, Waterloo, Ontario, Canada, in 1997, all in electrical engineering.

From 1990 to 1994, he was with Nanjing University of Aeronautics and Astronautics, China. He was with Com Dev Ltd., Cambridge, Canada, as an Advanced Member of Technical Staff in 1997. He spent six months each in 1998, first with the Gordon McKay Laboratory, Harvard University, Cambridge, MA, and then with the Radiation Laboratory, the University of Michigan, Ann Arbor, MI, as a Postdoctoral Fellow. In 1999, he joined Nanyang Technological University (NTU), Singapore, as an assistant professor. He has been an associate professor in the School of Electrical and Electronic Engineering, NTU, since Jan. 2004.

Dr. Shen is a member of the Antennas and Propagation and Microwave Theory and Techniques Societies of the IEEE. He served as Chair of the IEEE MTT/AP Singapore Chapter. He was as the Chair of AP-S Chapter Activities Committee from Jan. 2010 to Aug. 2014. He is currently serving as the Secretary of IEEE AP-S.

His research interests include design of small and planar antennas for various wireless communication systems, analysis and design of frequency-selective structures and absorbers, hybrid numerical techniques for modeling RF/microwave components and antennas. He has authored or co-authored more than 130 journal papers and presented another 120 conference papers.